Correlations between ferromagnetic-resonance linewidths and sample quality in the study of metallic ultrathin films

W. Platow, A. N. Anisimov, G. L. Dunifer,* M. Farle, and K. Baberschke
Institut für Experimentalphysik, Freie Universität Berlin, Arnimallee 14, D-14195 Berlin-Dahlem, Germany
(Received 12 January 1998)

Ferromagnetic resonance is commonly used in the study of thin ferromagnetic films. In past investigations, most attention has been concentrated on the resonance field H_r, with relatively little consideration for the information contained in the peak-to-peak linewidth ΔH_{pp}. In this paper we focus specifically on ΔH_{pp}, looking at a variety of Fe, Co, Ni, and Gd films (thickness <20 monolayers) epitaxially grown on different single-crystal substrates of various orientations, as well as an $Fe_4/V_4(100)$ multilayer. We identify common features in the linewidths which correlate with other film properties, such as intrinsic spin-damping mechanisms, and the structural and magnetic quality. The dependence of ΔH_{pp} on film thickness and annealing conditions, as well as temperature, frequency, and magnetic-field orientation is examined. Particularly interesting is an angular dependence of ΔH_{pp}, seen most clearly in Fe_4/V_4 which is related to the crystallographic axes and appears to be correlated with the intrinsic damping of the spins. [S0163-1829(98)02733-7]

I. INTRODUCTION

Ferromagnetic resonance (FMR) is one of the standard techniques often used in the study of magnetic thin films and multilayers (see, for example, Refs. 1–6). The vast majority of such FMR studies have concentrated on the magnitude of the resonance field H_r and its dependence on such variables as the field orientation, the sample thickness, the temperature, and so forth. Relatively little attention has been paid to the peak-to-peak linewidth of the resonant signal ΔH_{pp}. In this paper we focus specifically on FMR linewidths, gathering data from a variety of ultrathin films that were prepared, and in most cases measured *in situ*, under ultrahigh vacuum (UHV) conditions. The intent is to show that there are common features in the linewidths which provide important information about the sample, such as intrinsic damping mechanisms and the structural and magnetic quality. We will discuss in detail the various contributions which yield the experimentally measured FMR linewidths. One should note that Brillouin light scattering is capable of collecting similar information for different wave vectors of spin waves.[7] FMR primarily measures the lowest energy, that is the uniform-precession mode, $k=0$. We present experimental results for epitaxially grown Fe, Co, Ni, and Gd ultrathin films [thickness $d<20$ monolayers (ML)] grown on different single-crystal substrates with different orientations. We find that ΔH_{pp} is a very sensitive measure of the sample's structural and magnetic quality. In general, the narrowest linewidth is measured for layers with the best possible structural quality and purity as judged by low- and medium-energy electron diffraction (LEED, MEED) and Auger spectroscopy. ΔH_{pp}, which consists of homogeneous and inhomogeneous parts, depends on details of the sample preparation, on temperature, and film thickness. It is pointed out that the linewidth of different layers should be compared at the same reduced temperature T/T_C, since it is well known that the linewidth increases sharply near the Curie temperature T_C, which varies strongly with film thickness d.

For a more quantitative analysis in terms of intrinsic (homogeneous) and inhomogeneous contributions to the FMR linewidth, the angular and frequency dependence of selected samples was measured and analyzed using the phenomenological theories discussed in the literature. For example, in the case of tetragonal Ni(001) on Cu(001) we find an enhanced intrinsic damping of the magnetization in comparison to bulk Ni, which can be related to the increased importance of the spin-orbit interaction[3,4] and changes in the orbital moment in ultrathin films. Similar results were reported for bcc Fe on Ag(001).[8,9]

For completeness, we also include a discussion of the dependence of ΔH_{pp} on the direction of the applied dc magnetic field with respect to the crystallographic directions in the layer and with respect to the film plane. The measurement of the angular-dependent linewidth becomes a very sensitive tool to determine magnetic inhomogeneities due to local variations of magnetic anisotropy, film thickness, and magnetization. We show for nearly structurally perfect $(Fe_4/V_4)\times 40$ superlattice samples that measurements as a function of the orientation of the magnetic field in the film plane reveal a possible anisotropy in the intrinsic damping which can be related to the symmetry of the crystallographic structure. This again is related to the role of the spin-orbit interaction and orbital magnetic moments in ultrathin film structures with reduced (tetragonal) symmetry.

We believe it is worthwhile to mention that the FMR linewidth provides similar information on the relaxation time of the magnetization as was recently measured in a sophisticated study of the magnetization reversal using ultrashort (10^{-12} s) magnetic-field pulses.[10,11] These results have been successfully interpreted[12] using the well-known Landau-Lifshitz equation with an intrinsic Gilbert type of damping, which has been used in FMR for many years to determine the intrinsic relaxation rate in ferromagnets.

Our paper is organized as follows: We begin by summarizing the phenomenological approaches which have been used in the past to describe the angular and frequency depen-

0163-1829/98/58(9)/5611(11)/$15.00

dence of the experimental resonance linewidth. This is followed by a presentation and a qualitative discussion of the behavior of ΔH_{pp} as a function of temperature, film thickness, and thermal treatment which we measured in different Fe, Co, Ni, and Gd films.[13–18] Finally, we show for Ni/Cu(001) and a prototype system $(Fe_4/V_4)\times 40$ with nearly perfect structural quality how to obtain quantitative information on the homogeneous and inhomogeneous contribution from frequency- and angular-dependent FMR measurements.

II. PHENOMENOLOGICAL DESCRIPTION OF FMR

Below we review briefly some of the standard phenomenological theories and resulting equations that are commonly used in the literature for describing and interpreting FMR and linewidths. In previous studies, in which the linewidth was considered, it has been common to express it in the following form:

$$\Delta H_{pp}(\omega)=\Delta H_{\mathrm{inhom}}+\Delta H_{\mathrm{hom}}=\Delta H_{\mathrm{inhom}}+\frac{2}{\sqrt{3}}\frac{G}{\gamma^2 M}\omega, \tag{1}$$

where the experimental linewidth $\Delta H_{pp}(\omega)$ is taken as the peak-to-peak field variation in the signal (usually displayed as the derivative of a Lorentzian line shape). $\Delta H_{\mathrm{inhom}}$ describes an inhomogeneous broadening due to sample imperfections (assumed independent of the applied frequency ω), and ΔH_{hom} is the intrinsic linewidth that would occur in a perfect sample (assumed linearly proportional to the frequency ω). As indicated, ΔH_{hom} may be expressed in terms of the Gilbert damping parameter G in the Landau-Lifshitz equation and the saturation magnetization M of the ferromagnetic material. By measuring the FMR signal at two or more frequencies, it is then possible to plot $\Delta H_{pp}(\omega)$ as a function of the frequency and thereby extract G from the slope of the curve and $\Delta H_{\mathrm{inhom}}$ from the intercept.[8] However, as we will show, both from experimental data and also from solutions of the Landau-Lifshitz equation, one must proceed cautiously in carrying out this procedure. This is because for general orientations of the magnetization and magnetic field:

(a) ΔH_{hom} is *not* always linearly proportional to the frequency ω,

(b) $\Delta H_{\mathrm{inhom}}$ is *not* always independent of the frequency, and

(c) G may *not* be an absolute constant, but may vary as the applied field and magnetization are rotated with respect to the sample geometry.

It is generally believed[19] that the spin-orbit interaction in the ferromagnet plays a dominant role in the damping mechanism, as well as determining the Landé g factor. As shown by Elliott,[20] this leads to the following approximate relationship:

$$G\propto\Delta g^2, \tag{2}$$

where Δg is the deviation of the Landé g factor from the free-electron value 2.0023.

Below, we show data for thin films and multilayers having several different crystal structures and orientations. Most of our attention will be on tetragonal crystal structures with a [001] orientation normal to the film plane. In such samples, angular-dependent measurements of the resonance field H_r and the linewidth ΔH_{pp} were performed with the dc magnetic field $\mathbf{H}$ rotated: (a) in the film plane by varying the azimuthal angle ϕ_H, measured from the [100] crystal axis, and (b) out of the film plane as a function of the polar angle θ_H, measured from the [001] axis (film normal) to the [110] axis (in the film plane). The orientation of the magnetization $\mathbf{M}$ is expressed in terms of the angles ϕ and θ, measured relative to the same crystalline axes.[21–23] In terms of these angles, the anisotropic part of the free energy density (MAE) for a tetragonal system to fourth order is

$$F=-HM[\sin\theta\,\sin\theta_H\cos(\phi-\phi_H)+\cos\theta\,\cos\theta_H]+(2\pi M^2-K_2)\cos^2\theta-\tfrac{1}{2}K_{4\perp}\cos^4\theta-\tfrac{1}{8}K_{4\parallel}(3+\cos 4\phi)\sin^4\theta. \tag{3}$$

Each of the above anisotropy constants K_i $(i=2,4)$ can be expressed in the following form for a thin film (see, for example, Ref. 24):

$$K_i=K_i^v+\frac{2K_i^s}{d}, \tag{4}$$

where d is the film thickness in monolayers, K_i^v is a thickness-independent contribution, and K_i^s/d is a thickness-dependent contribution due in part to the lowered coordination at the substrate/film or film/vacuum interface.[25,26] The equilibrium orientation of the magnetization vector $\mathbf{M}$ is defined by the angles θ_0 and ϕ_0, which are obtained, respectively, from the equations:

$$F_\theta\equiv\partial F/\partial\theta=0;\quad F_\phi\equiv\partial F/\partial\phi=0. \tag{5}$$

The Landau-Lifshitz equation with damping has the form:

$$\frac{dM}{dt}=-\gamma\mathbf{M}\times\mathbf{H}+\frac{G}{\gamma M^2}\left[\mathbf{M}\times\frac{d}{dt}\mathbf{M}\right], \tag{6}$$

where G is the Gilbert damping factor. From Eq. (6) neglecting damping, the standard condition for resonance becomes[21]

$$\omega=\frac{\gamma}{M\,\sin\theta_0}\{F_{\theta\theta}F_{\phi\phi}-F_{\theta\phi}^2\}^{1/2}, \tag{7}$$

where the double subscipts refer to the second partial derivatives of the free energy density [Eq. (3)] with respect to the indicated angles. For $\mathbf{H}$ perpendicular or parallel to the film plane, Eqs. (3) and (7) lead to the well-known Kittel resonance conditions:

$$\frac{\omega}{\gamma}=H_{r\perp}-4\pi M+\frac{2(K_2+K_{4\perp})}{M}\quad(H\perp\ \text{film plane}), \tag{8}$$

$$\left(\frac{\omega}{\gamma}\right)^2=\left(H_{r\|}-\frac{2K_{4\|}}{M}\right)\left(H_{r\|}+4\pi M-\frac{2K_2}{M}+\frac{K_{4\|}}{M}\right)$$

$$(H\|[110] \text{ in film plane}). \tag{9}$$

For an arbitrary angle θ_H, the resonant condition is given by Eq. (3) in the paper by Farle *et al.*[23] With the Gilbert damping term in Eq. (6), the solution for the general resonant condition, Eq. (7), also leads to the following expressions for the intrinsic linewidth of the resonance:[21]

$$\Delta H_{\mathrm{hom}}=\frac{1}{\sqrt{3}}\frac{1}{|\partial\omega/\partial H|}\frac{G}{M^2}\left(F_{\theta\theta}+\frac{F_{\phi\phi}}{\sin^2\theta}\right) \tag{10}$$

$$\approx\frac{2}{\sqrt{3}}\frac{G}{\gamma^2 M}\frac{\omega}{\cos(\alpha-\alpha_H)}, \tag{11}$$

where α and α_H represent ϕ and ϕ_H for in-plane rotations[27] and θ and θ_H for out-of-plane rotations of the applied field. For out-of-plane rotations, we have verified Eq. (11) numerically for our sample parameters by computer simulations using Eqs. (3) and (5). And, finally, if a nonideal sample consists of a network of regions having slightly different orientations and physical characteristics, a common way of representing $\Delta H_{\mathrm{inhom}}$, patterned after the form used by Chappert *et al.*[28] for rotations in θ_H, is given by the expression:

$$\Delta H_{\mathrm{inhom}}=\left|\frac{\partial H_r}{\partial\theta_H}\right|\Delta\theta_H+\left|\frac{\partial H_r}{\partial\phi_H}\right|\Delta\phi_H+\left|\frac{\partial H_r}{\partial H_{\mathrm{int}}}\right|\Delta H_{\mathrm{int}}, \tag{12}$$

where $\Delta\theta_H$ and $\Delta\phi_H$ represent the spread in the orientations of the crystallographic axes among the various regions, and ΔH_{int} is related to the inhomogeneity of the internal magnetic fields throughout the specimen. As defined by Chappert *et al.*, $H_{\mathrm{int}}=4\pi M-2(K_2+K_{4\perp})/M$, and inhomogeneities in this quantity make their most significant contribution to the linewidth as **M** approaches the sample normal.

III. TEMPERATURE- AND THICKNESS-DEPENDENT FMR LINEWIDTHS

In this section we give an overview of the thickness- and temperature-dependent peak-to-peak linewidths of Fe, Co, and Ni ultrathin ($d<20$ ML) films on Cu(001), and of Gd(0001) and Ni(111) on W(110). All samples were prepared and measured *in situ* in UHV. Details of our FMR-UHV apparatus[29] and of the film characterization by LEED, MEED, and Auger spectroscopy have been reported previously.[23,30] The temperature and thickness dependence of the magnetic anisotropy energy (MAE) for Ni/Cu(001), Gd(0001)/(W110), and Ni(111)/W(110) was reported, for example, in Refs. 23 and 30–32. Results on the behavior of the resonance linewidth near the Curie temperature of Ni(111)/W(110) were presented in Ref. 14. Here we will present results only on the FMR linewidth which were not published before.

As mentioned in the Introduction, it is generally observed that the narrowest peak-to-peak linewidth is observed for samples which have the best structural quality. As an example, we consider the prototype system Ni/Cu(001). I(E)-LEED measurements have shown[33] that a nearly ideal tetragonal Ni crystal grows in perfect registry with the Cu(001) substrate at least up to 10 ML. The FMR spectra of a 7.2 ML Ni/Cu(001) film measured at 297 K *in situ* at three different microwave frequencies (Fig. 1) confirm this structural result. Here we measure the smallest inhomogeneous contribution to the linewidth ever reported for a metallic Ni sample (see Table I). In some FMR studies high microwave frequencies (37, 70 GHz) were used. It is obvious from Fig. 1 that for a ΔH_{pp} analysis, the lower microwave frequencies allow a more accurate determination of $\Delta H_{\mathrm{inhom}}$. The inset of Fig. 1 shows the three experimental linewidths ΔH_{pp} as a function of the frequency. We find the expected linear dependence [Eq. (1)] with an almost negligible inhomogeneous contribution $\Delta H_{\mathrm{inhom}}$. This indicates that the magnetic inhomogeneities due to local variations of the magnetization and anisotropy constants [Eq. (9)] are very small. Note, this also implies that, even if there are large relative variations (say 20%) of K or M across the film due to inhomogeneities, the inhomogeneous broadening may be reduced if the mean value of M or K is small, in other words the inhomogeneous linewidth of a 20% variation of $K=100$ μeV/atom is absolutely much larger than for $K=1$ μeV/atom. The experimental linewidth (Fig. 1) $\Delta H_{pp}=250$ Oe (at 9 GHz) is almost exclusively due to intrinsic damping.

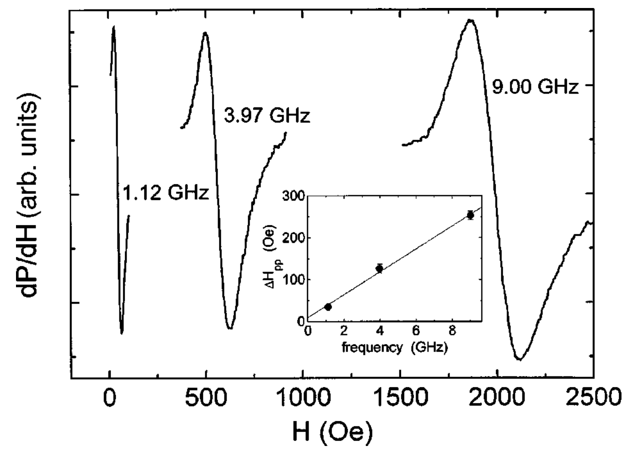

FIG. 1. Typical experimental FMR spectra of 7.2 ML Ni/Cu(001) at three different frequencies recorded at 297 K. The external magnetic field is applied in the film plane parallel to the [110] direction. Note the shift to lower resonance fields and the decrease of ΔH_{pp} with decreasing frequency. Inset: Frequency dependence of ΔH_{pp}.

Here we would like to point out the very good signal-to-noise ratio observed at all three frequencies (even at 1 GHz), which allows the precise determination of ΔH_{pp}. FMR spectra of such quality have been observed in our experiments only when the roughness across the total extent of the film (about 18 mm^2) is small on an atomic scale, that is to say, when the film surface has only monoatomic steps. Another important point concerns the layerwise structural homogeneity. If the structure changes as a function of thickness, an inhomogeneous broadening of the resonance linewidth is observed, as for example, in the case of Co/Mn superlattices.[34]

However, care must be taken, if one wants to draw conclusions on the magnetic and structural quality of different

TABLE I. A summary of the narrowest linewidths measured at 9 GHz and $(0.6\pm0.1)T_C$. For comparison, we also list bulk data, the Gilbert parameter G, and the calculated ΔH_{hom} according to Eq. (1) using the bulk magnetization $M(T/T_C=0.6)$ of the respective elements.

	$\Delta H_{pp}^{\mathrm{exp}}$ (Oe)	G (10^8 s^{-1})	ΔH_{hom} (Oe)
6.3 ML Ni/Cu(001) [a]	185	5.5 ± 0.3	200
12.5 ML Ni/W(110) [b]	310		
Ni bulk	130 (Ref. 38)	2.5 (Ref. 41)	91
2.3 ML Co/Cu(001)	215		
Co bulk	110 (Ref. 38)	3 (Ref. 50)	40
2.8 ML Fe/Cu(001)	210		
$(\mathrm{Fe}_4/\mathrm{V}_4)_{40}$ ($H\Vert[110]$)	36	1.5–2.2	25–36
Fe bulk	32 (Ref. 38)	0.58 (Ref. 9)	6.9
30 ML Gd/W(110)	110		
Gd bulk	340 (Ref. 51)	2 (Ref. 3)	24

[a]For this sample $\Delta H_{\mathrm{hom}} > \Delta H_{pp}^{\mathrm{exp}}$. The uncertainties in G are almost sufficient to reverse the inequality. This implies $\Delta H_{\mathrm{inhom}}$ is very small and the film quality is high.
[b]Measured at $T=0.9T_C$.

samples from FMR-linewidth measurements. As seen in Figs. 2 and 3, the linewidth depends on temperature and the thickness of the epitaxial film. In general, three characteristic features are observed which will be discussed below: (a) a large linewidth near T_C, (b) a shallow minimum below T_C, and (c) an overall larger linewidth for thinner films deep in the ferromagnetic regime. Near the Curie temperature $T_C(d)$ (indicated by the arrows in Fig. 2) a strong increase of ΔH_{pp} is observed, which is due [Eq. (1)] to the disappearance of the magnetization $M(T)$. The intrinsic (homogeneous) contribution to the linewidth shows a maximum, as discussed previously.[14] Here we do not want to discuss this feature near T_C in detail, but only to point out that except for the data in Fig. 2(a) and for our own Ni(111) study,[14,35] there exists only one other FMR measurement on a metallic bulk sample[36] where a clear peak in ΔH_{pp} near T_C was observed. The observation of such a peak in Fig. 2 shows again that thin ferromagnetic layers grown under UHV conditions are

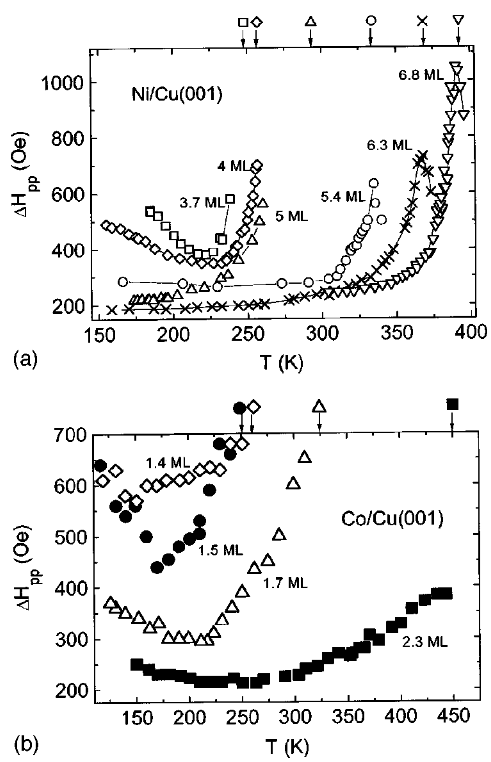

FIG. 2. Temperature dependence of ΔH_{pp} in (a) Ni/Cu(001) (Ref. 16) and (b) Co/Cu(001) (Ref. 13) monolayers measured at 9 GHz with **H** parallel to the in-plane [110] direction. The solid lines are guides to the eye. The arrows at the top indicate the Curie temperature for each film.

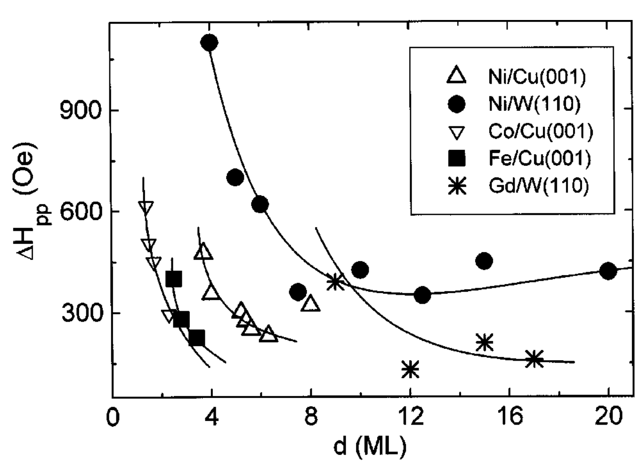

FIG. 3. Thickness dependence of ΔH_{pp} for five different systems at the same reduced temperature $T/T_C(d)=0.8$ measured at 9 GHz with **H** parallel to the in-plane [110] direction. The solid lines serve as a guide to the eye. Data are taken from Refs. 13, 16, 18, and 40.

in general more perfect crystals than bulk lattices. For example, in Ref. 36 a prolonged and sophisticated annealing procedure had to be performed on carefully polished spherical Ni samples to see the maximum in ΔH_{pp} at T_C. A similar increase of ΔH_{pp} is seen in the case of Co/Cu(001) [Fig. 2(b)]. Unfortunately, the maximum in ΔH_{pp} cannot be resolved for the thinner layers, since the FMR signal, which is proportional to $M(T)$, decreases below the sensitivity limit of our apparatus. In the case of Co/Cu(001), morphological imperfections[37] (for $d<2$ ML) may also play a role.

In general, below the Curie temperature we find a shallow minimum of ΔH_{pp} at around 0.7 to 0.8 $T_C(d)$ [Figs. 2(a) and 2(b)]. Note, that one should use the thermodynamically relevant parameter, i.e., the reduced temperature $T/T_C(d)$, to compare ΔH_{pp} at different thicknesses. Qualitatively, the increase of the linewidth at lower temperature can be understood as an inhomogeneous broadening. It is known that the anisotropy constants are strongly temperature dependent[26,38] and increase with decreasing temperature.[39] A variation of say 1% causes a larger inhomogeneous linewidth at lower T than closer to T_C.

In Fig. 3 we show the general thickness dependence of the FMR linewidth. The narrowest linewidths of several thin-film systems [taken at $0.8T_C(d)$] recorded at 9 GHz with the magnetic field parallel to the film plane [Eq. (9)] is shown. Below a certain thickness d_c, which depends on the system, a strong increase of the linewidth, up to a factor of 3, is observed. One might attempt to attribute this increase to inhomogeneous broadening as a result of the increased importance (proportional to $1/d$) of the interface anisotropy K_i^s according to Eqs. (4) and (9). This explanation, however, does not work universally, as H_r has considerably different dependences on d in the various systems—sometimes increasing and sometimes decreasing as d is reduced. As an example, a simple estimate with the known anisotropy value of $K_2(0.8T_C)$ for Ni/Cu(001),[26,39] assuming a variation of $\Delta K_2^s/K_2^s = 2\%$, we find that $\Delta H_{\mathrm{inhom}}$ decreases by a factor of 4 between 6 and 3 monolayers. This is in the opposite direction necessary to account for the behavior displayed in Fig. 3 and is due primarily to the rapid decrease in H_r as d is reduced. From Eq. (9), neglecting the small contribution from $K_{4\parallel}/M$ (appropriate for the Ni/Cu system), we find

$$\frac{\Delta H_r}{\Delta K_2^s} = \frac{H_r}{d[\pi M^2 + 1/2(MH_r - K_2^v)] - K_2^s}. \qquad (13)$$

For $d<6$ ML, the denominator of Eq. (13) is dominated by the K_2^s term, and the H_r factor in the numerator primarily determines the thickness dependence of a $\Delta H_{\mathrm{inhom}}$ due to a spread of K_2^s values. Thus, for the Ni/Cu system a small spread of K_2^s values over the sample can be ruled out as the source of the linewidth broadening in the thinnest specimens. Only a very rapid increase in ΔK_2^s with decreasing thickness could account for the observed broadening. Using Eq. (9) similar statements can be made in regard to contributions to $\Delta H_{\mathrm{inhom}}$ from a spread of M or K_2^v values.

Another possible explanation is the change in dimensionality from three to two dimensions, which occurs in the case of Ni/W(110) around 5–6 ML.[14] In this model the increase is due to a homogeneous broadening which results from an enhanced scattering of the zero-wave-vector spin wave (i.e., the FMR) due to the larger extent of magnetic fluctuations in the quasi-two-dimensional film. Frequency-dependent measurements, which would distinguish both contributions, were not possible for many of our ultrathin films, because either the resonance vanished at the lowest frequency or the sensitivity was not sufficient. In some cases, both effects (dimensionality and inhomogeneities in the magnetic constants) may contribute to the increase of ΔH_{pp} as, for example, was determined in the case of Fe/Ag(001).[9]

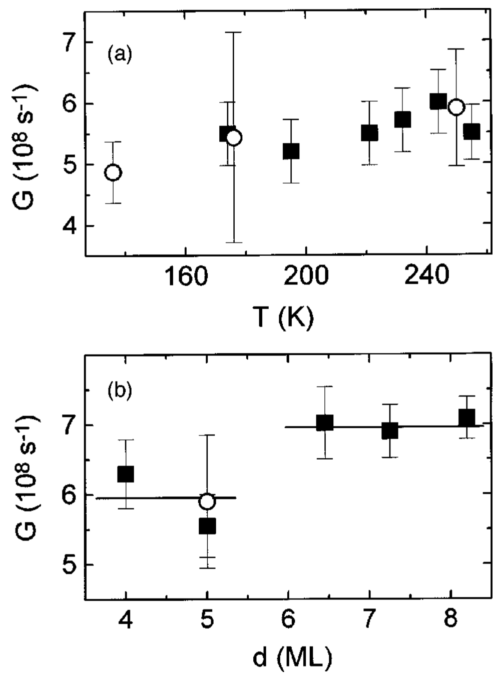

FIG. 4. (a) Temperature dependence and (b) thickness dependence of the Gilbert damping parameter of uncapped 5 ML Ni/Cu(001) (solid squares) and capped with 5 ML Cu (open circles). **H** is applied along the in-plane [110] direction. The thickness dependence is taken between 240 and 300 K. The solid lines serve as a guide to the eye. It was not possible in all cases to make a measurement at the three frequencies, which resulted in larger error bars.

In the case of Ni/Cu(001), a thickness-, temperature-, and frequency-dependent study was performed to distinguish the homogeneous and inhomogeneous contribution [Eq. (1)] to $\Delta H_{pp}(T,d)$. The Gilbert damping parameter [Eq. (1)] was determined [Figs. 4(a) and 4(b)] from measurements at 1, 4, and 9 GHz with the magnetic field applied in the film plane. First, one notices that G for 5 ML Ni/Cu(001) does not depend on temperature within the scatter of the data [Fig. 4(a)] and does not change when capping the film with a Cu layer. Also, in bulk Ni (Refs. 4 and 41) and Fe films on Ag(001),[36] G was found to be temperature independent in this temperature range. Interestingly, G of the thin Ni film is larger by a factor of 2 than the generally quoted value of bulk Ni ($G = 2.5\times 10^8\ \mathrm{s}^{-1}$).[41] The reason for this enhancement is most likely the reduced dimensionality and the increased importance of spin-orbit interaction in the tetragonal film (in comparison to cubic bulk Ni).[9,19,42]

Interestingly, there appears to be a decrease of G for Ni/Cu(001) [Fig. 4(b)] when the thickness is reduced from about 7 to 5 ML. Consequently, the increase of ΔH_{pp} below

5 ML (Fig. 3) should be due to some form of inhomogeneous broadening or dimensionality effects which do not affect G, as discussed before. This is opposite to the behavior reported for Fe/Ag(001), where G was found to increase by almost a factor of 10 for smaller thickness.[9] A simple interpretation cannot be given. One may consider, however, that around 7 ML a thickness-dependent continuous reorientation of the magnetization from perpendicular ($d>8$ ML) to in-plane ($d<7$ ML) occurs.[22,43] Two possible effects on G may be discussed: (a) In the transition range (7–8 ML) the intrinsic damping may be enhanced due to fluctuations of the order parameter at the transition. Additional experiments at larger thickness would be needed to verify this interpretation. (b) The change in G may reflect the intrinsic anisotropy of the tetragonal lattice. All measurements were performed with the magnetic field applied in the film plane, that is to say, for $d>7$ ML along a hard and for $d<7$ ML along the easy direction of magnetization. The difference in G between easy and hard directions is similar to the case of fcc Co,[19] where the larger $G=2.8\pm0.3\times10^8$ rad/s is found for measurements with **H** along the hard direction compared to $G=1.7\pm0.2\times10^8$ rad/s for **H** along the easy axis. Later in Sec. IV we will show for a Fe_4/V_4 multilayer that G depends strongly on the orientation of **M**. An anisotropic Gilbert term (up to 30% variation) was also reported in the case of Fe films.[8] In this case, however, a larger value for G was obtained with **H** along the easy axis. The origin of such a large anisotropic G in distorted layers could be related to the presence of an anisotropic orbital momentum, which yields an anisotropic g factor.[25] And, according to Eq. (2), this should be reflected in G. However, to answer the question why the larger G is found for **H** along the easy axis in bcc Fe/Ag(001) and along the hard axis in Co/Cu(001) needs further investigation.

Now we discuss the angular dependence of the resonance linewidth. As an example, we show in Fig. 5 the dependence of ΔH_{pp} on the angle θ_H for 7.6 ML Ni/Cu(001) as measured at 9 GHz at three different temperatures. For this film the magnetization changes from in-plane to out-of-plane with increasing temperature,[43] as indicated in the figure. Because this film is experiencing a reorientation transition, the anisotropy fields are quite well balanced, and H_r varies by only a few hundred Oe with the rotation of the field direction.[23] In general, ΔH_{pp} is largest for $\theta_H=0°$, and passes through a minimum for θ_H in the range of 50°–60° at all three temperatures. In the previous discussion [concerning Fig. 4(b)] it was suggested that the Gilbert parameter is larger for H along the hard direction. Thus, as the temperature is raised, and the easy axis changes, one would expect $\Delta H_{pp}(\theta_H=0°)$ to continuously decrease and $\Delta H_{pp}(\theta_H=90°$, in-plane) to increase. The data, however, do not appear to show this behavior, implying that for this sample a significant inhomogeneous contribution may also be present. As an attempt to fit the data, we have used the method of Chappert *et al.*,[28] in which the angular dependence of ΔH_{pp} can be represented by the first and third terms on the right side of Eq. (12) plus a constant term ΔH_0. This constant term can be thought of as the homogeneous contribution for the case $\theta\approx\theta_H$ in Eq. (11). The solid lines in Fig. 5 are the result of this fitting procedure using the parameters given in the figure caption. As can be seen, the experimental data curves can be fairly well reproduced, however, the required values for $\Delta\theta_H$, ΔH_{int}, and ΔH_0 display considerable scatter for the different temperatures, a behavior which is not easily interpreted. Furthermore, there is no obvious reason why this sample, which is very similar to the one displayed in Fig. 1, should have such a large $\Delta H_{\mathrm{inhom}}$, while the one in Fig. 1 had almost no contribution from $\Delta H_{\mathrm{inhom}}$ to the linewidth at 9 GHz. We thus consider this fitting procedure unreliable, even though at any one temperature it is able to fit the angular dependence of the linewidth data quite well. A more rigorous (and we believe reliable) procedure will be used to fit the angular dependence of ΔH_{pp} for the Fe_4/V_4 multilayer discussed in the next section.

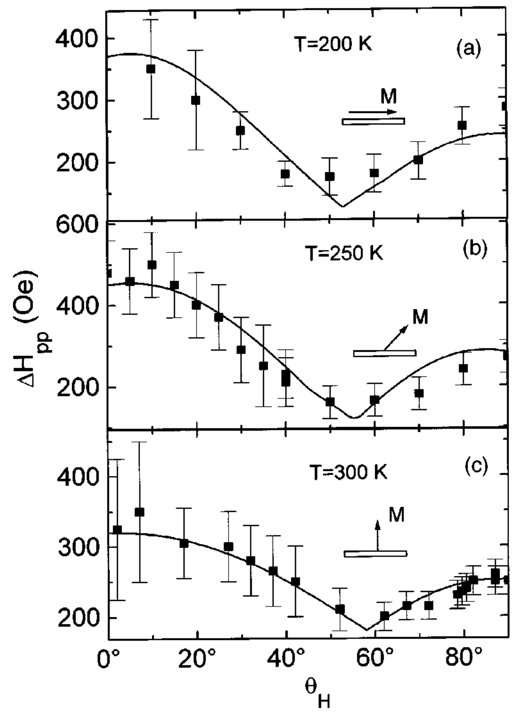

FIG. 5. ΔH_{pp} as a function of θ_H for 7.6 ML Ni/Cu(001) at three different temperatures recorded at 9 GHz. θ_H is the polar angle measured from the [001] axis to the [110] axis. The easy axis of the magnetization rotates from (a) in-plane to (c) out-of plane by increasing the temperature. Note the different scales on the vertical axes. The solid line is a fit to the experimental data according to the method of Chappert *et al.* (Ref. 28) with the parameters: ΔH_{int}, $\Delta\theta_H$, $\Delta H_0=$(a) 250 Oe, 1°, 120 Oe, (b) 350 Oe, 5°, 100 Oe, (c) 150 Oe, 1°, 170 Oe.

For completeness, we mention a related approach discussed by Cochran *et al.*,[44] in which there is assumed a spread of K_2 and K_4 values around some mean value. One can see from Eqs. (8) and (9) that a distribution of K_i will result in different inhomogeneous broadenings for in-plane and out-of-plane measurements. Using this approach, a minimum in the resonance linewidth at intermediate angles can also be calculated for the range of anisotropy values present in our samples.

Finally, we would like to give an illustrative example that ΔH_{pp} is indeed related to structural and morphological changes in a clean ultrathin film. In Fig. 6 we show the temperature dependence of ΔH_{pp} for a 17 ML Gd(0001)/W(110) film at three successive stages of preparation: (a) as deposited at 300 K, (b) after heating to 480 K, and (c) after

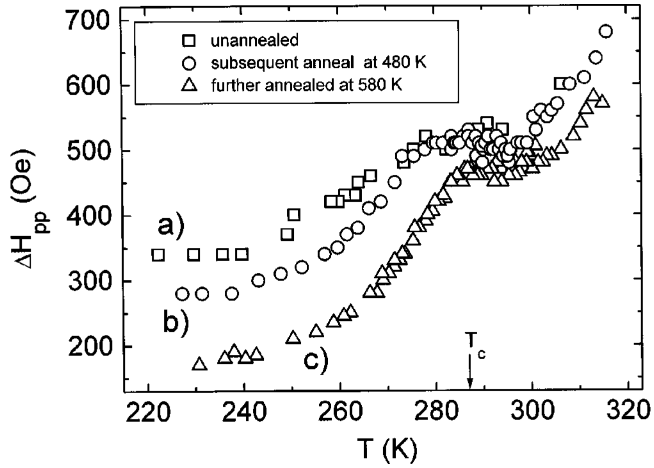

FIG. 6. Temperature dependence of ΔH_{pp} for 17 ML Gd/W(110) measured (a) before annealing, (b) after subsequent annealing to 480 K and (c) after annealing to 580 K (Ref. 18).

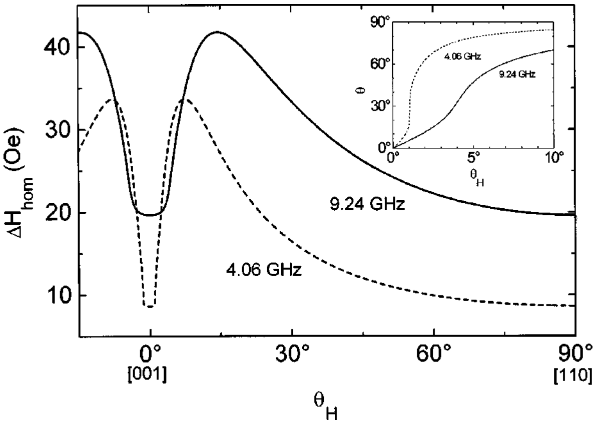

FIG. 7. The intrinsic contribution to the linewidth versus θ_H as calculated from Eq. (10) using $G=1.18\times 10^8$ rad/s and the other parameters listed in the text. Inset: The orientation of the magnetization **M** versus θ_H as calculated from Eq. (5).

heating to 580 K. This thermal treatment of the layer-by-layer grown film sharpens the initially diffuse LEED pattern considerably and strongly increases the magnitude of the susceptibility at $T_C=288$ K. The latter is correlated to the improved magnetic homogeneity.[45] ΔH_{pp} at $0.8T_C$ decreases successively by almost a factor of 2 during this treatment (from 350 to 180 Oe). This shows that structural homogeneity is strongly correlated with ΔH_{pp}. After the 580 K anneal, the layer is found to be smooth and structurally the most homogeneous.[45,46] Heating to the still higher temperature of 870 K changes the film's morphology. Large flat islands with thickness $d>30$ ML are most likely formed, which agglomerate on top of a 1 ML Gd/W(110).[17,45,46] This results in a broadening of the resonance linewidth due to a distribution of effective internal anisotropy and demagnetization fields.[17] Interestingly, this inhomogeneous broadening, due to island formation, yields the same ΔH_{pp} as was found for the smooth, but structurally ill-defined, as-deposited film.

IV. AN Fe_4/V_4 MULTILAYER CASE STUDY

As a case study, we consider the FMR spectra of an exceptionally high-quality $Fe_4/V_4(001)$ superlattice specimen grown on a MgO(001) substrate in an UHV-based sputtering system. X-ray-diffraction studies have shown the sample has both high structural and interfacial quality.[47] The sample has 40 superlattice periods with a modulation wavelength of 1.177 nm. The easy magnetization axis lies in-plane along a [100] direction. The FMR measurements described here were carried out at room temperature at the two frequencies 4.06 and 9.24 GHz. Earlier reports[48,49] have described the MAE of this sample plus its temperature dependence. As reported there, the dependence of the resonance field H_r on the orientation of the applied magnetic field is well described by the following parameters used in expressing the free energy density to fourth order [see Eq. (3)]: $g=2.09$, $2\pi M-K_2/M=6.25$ kOe, $K_{4\parallel}/M=0.032$ kOe, and $K_{4\perp}/M=-0.615$ kOe.

First, we consider the characteristics of the FMR signal for rotation of the magnetic field through θ_H (out of the film plane). In Fig. 7 we plot ΔH_{hom} versus θ_H for the two frequencies of our study, as calculated from Eq. (10) for our sample parameters. For the Gilbert damping factor we have arbitrarily used $G=1.18\times 10^8$ rad/s, among the typical values quoted in the literature for Fe. For each frequency, ΔH_{hom} is the same at $\theta_H=0°$ and 90°. At intermediate angles the linewidth is larger. This is because of the $\cos(\theta-\theta_H)^{-1}$ factor in Eq. (11). Because the magnetization easy axis lies in the plane of the specimen, as the magnetic field **H** is rotated out of the plane, the magnetization **M** lags behind, until a fairly large angle develops between the two vectors. The maximum separation of **M** and **H** occurs for $\theta_H\approx 10°$ to 20°, depending on the frequency. The inset of the figure shows the orientation of **M** for $0°\leqslant\theta_H\leqslant 10°$ as calculated from Eq. (5). As can be seen, there is a strong frequency dependence, with **M** remaining much closer to the film plane, for the smaller magnetic field associated with the lower frequency, until **H** becomes very close to the sample normal ($\theta_H=0°$). From Fig. 7 we see that ΔH_{hom} is proportional to the frequency ω only for the angles $\theta_H=0°$ and 90°, when **M** and **H** are parallel. In general, when **M** and **H** are not parallel, ΔH_{hom} is *not* linearly proportional to the applied frequency, as assumed in Eq. (1). In fact, as can be seen in the figure, there is a small angular range, $\theta_H\approx 3°-7°$, where ΔH_{hom} is actually larger at the lower frequency.

For rotations of the applied field out of the sample plane, the major angular-dependent contributions to $\Delta H_{\mathrm{inhom}}$ is the term $|\partial H_r/\partial\theta_H|\Delta\theta_H$ from Eq. (12). In Fig. 8 we display the θ_H dependence of H_r for the two observation frequencies. The circles correspond to experimental data, and the lines correspond to the simulation from Eqs. (3) and (7) for the given parameters. The agreement between the data and the resonance condition from the fourth-order energy density is good at both frequencies. The peak at $\theta_H=0°$ is considerably sharper at the lower frequency, because of the tendency of **M** to remain closer to the sample plane until θ_H is very close to 0°. The inset of Fig. 8 shows $|\partial H_r/\partial\theta_H|$ as calculated from the simulations at the two frequencies for $-2°\leqslant\theta_H\leqslant +10°$. The curve for the lower frequency was actually calculated as $|\Delta H_r/\Delta\theta_H|$ using a step size of $\Delta\theta_H=0.1°$. We have done this because the slope of the lower-frequency curve in Fig. 8 becomes so steep near $\theta_H\approx\pm 1°$

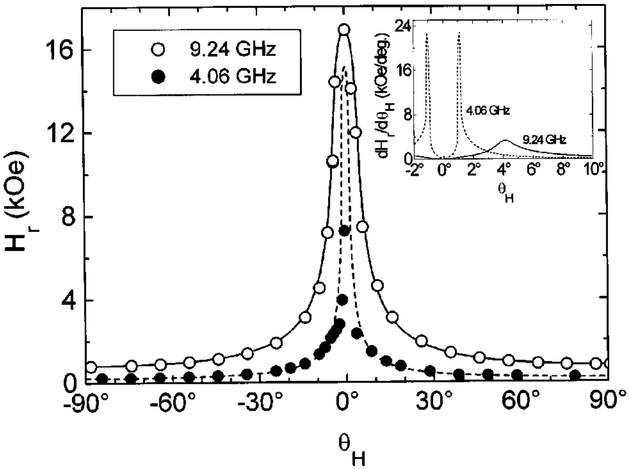

FIG. 8. The resonance field versus θ_H for the two observation frequencies. The circles represent the experimental data, and the lines are the simulations calculated from Eq. (7). Inset: The slope of the resonance field versus θ_H curve for the two observation frequencies. As explained in the text, the lower-frequency curve was calculated using a step size of $\Delta\theta_H = 0.1°$.

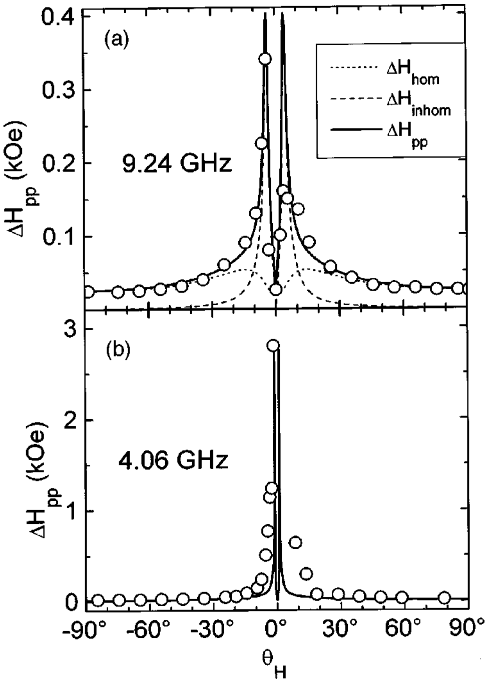

FIG. 9. The peak-to-peak linewidth as a function of θ_H. The circles give the experimental data, and the solid line is fitted by summing Eqs. (10) and (12), using the parameters: $G/M = 1.26 \times 10^5$ rad/s G, $\Delta\theta_H = 0.12°$, and $\Delta H_{\rm int} = 3$ Oe. (a) Results at 9.24 GHz. The dotted line is the homogeneous contribution, and the dashed line is the inhomogeneous contribution. (b) Results at 4.06 GHz.

that the variation of $\Delta\theta_H$ over the sample is unable to resolve the actual derivative. It should be noted from the inset of Fig. 8 that for a fixed value of θ_H (other than $\theta_H = 0°$), $\Delta H_{\rm inhom}$ will *not* be independent of the frequency, as assumed in Eq. (1). Once again, this situation occurs when **M** and **H** are not parallel.

Comparing the curves in Fig. 7 and the inset of Fig. 8, there is seen a similar angular dependence to the two linewidth contributions $\Delta H_{\rm inhom}$ and $\Delta H_{\rm hom}$. The contribution to $\Delta H_{\rm inhom}$, however, is a more sharply peaked function whose maximum is situated 3–5 times closer to $\theta_H = 0°$ than occurs for $\Delta H_{\rm hom}$. In Fig. 9 we have fitted the FMR linewidth data for rotations of θ_H using contributions from both $\Delta H_{\rm inhom}$ [Eq. (12)] and $\Delta H_{\rm hom}$ [Eq. (10)]. The sharp peaks in the data near $\theta_H = 0°$ are due primarily to the $|\partial H_r/\partial\theta_H|\ \Delta\theta_H$ term in Eq. (12). The fitting procedure is carried out most reliably for the 9 GHz data [Fig. 9(a)], where the angular variation is not so fast. The fit here requires a spread of $\Delta\theta_H = 0.12°$ among the various regions of the sample. This is consistent with the x-ray data.[47] To fit the data in the region $\theta_H \approx \pm 10°–50°$, it is necessary to have a contribution from $\Delta H_{\rm hom}$. The fitting procedure of Chappert *et al.* utilized a constant quantity ΔH_0 to represent $\Delta H_{\rm hom}$, and this often left a distinct gap between the data and the fitted curve in this angular range [e.g., see Figs. 3, 4, and 5 in their paper]. We have selected the value of G/M to optimize the fit near $\theta_H = \pm 90°$. Note that we do not need a constant term ΔH_0 in fitting the data. The individual contributions of $\Delta H_{\rm hom}$ and $\Delta H_{\rm inhom}$ are depicted in the figure. Vibrating-sample magnetometry measurements on this sample give at room temperature a magnetization $M = 1.192$ kOe, from which we obtain $G = 1.50 \times 10^8$ rad/s from our fitting procedure. The term $|\partial H_r/\partial H_{\rm int}|\Delta H_{\rm int}$, in Eq. (12) is a sharply peaked feature, centered at $\theta_H = 0°$ and only a few degrees in width. We have selected $\Delta H_{\rm int}$ in this term in order to fit the data at $\theta_H = 0°$. Our value for G is 2.6 times that measured in the bulk,[9] while the value determined for $\Delta H_{\rm int}$ is exceptionally small, once again indicative of the high quality of this specimen.

In Fig. 9(b) the same fitting procedure is shown for the data at 4 GHz using the same values for G/M, $\Delta\theta_H$, and $\Delta H_{\rm int}$. Although the maximum and minimum linewidths are well fitted by this procedure, the simulation is more sharply peaked near $\theta_H = 0°$ than the data. The linewidth data change so rapidly near $\theta_H = 0°$ that it was not possible to follow the dependence exactly. The individual data points are only accurate to about $\pm 1°$ in θ_H, which is insufficient resolution to show all the detail in the simulation. For example, the sharp dip in the simulation at $\theta_H = 0°$ was not observed. This absence could also be accounted for by a small tilt of the sample plane from a vertical plane by as little as 1°. Nevertheless, there still remains some discrepancies between experiment and simulation in the vicinity of $\theta_H = 0°$ which cannot be accounted for by our fitting procedure.

Next, we consider rotations of the field **H** in the sample plane (variation of ϕ_H with $\theta_H = 90°$). In this geometry, the solution of Eq. (5) shows that $K_{4\parallel}/M$ is sufficiently small that **M** simply follows **H** for all values of ϕ_H. Thus, $\phi = \phi_H$, and **M** and **H** are always parallel. As expected in this situation, Eq. (10) gives us a value for $\Delta H_{\rm hom}$ which is independent of ϕ_H, linearly proportional to the frequency ω, and in agreement with Eqs. (11) and (1). As shown in Fig. 3 of Anisimov *et al.*,[49] H_r has a total variation of about 100 Oe with the rotation in ϕ_H, with the resonance occuring at the highest fields for $\phi_H = 45°$, 135° (the in-plane hard axes) and at the lowest fields for $\phi_H = 0°$, 90° (the easy axes). A very small difference in H_r between observations at $\phi_H = 0°$

([100] axis) and $\phi_H=90°$ ([010] axis), was explained in terms of a small in-plane uniaxial anisotropy (a finite $K_{2\parallel}$), most likely arising from a step-induced anisotropy. As shown in that figure, one obtains a good fit between the data and the simulation for the ϕ_H dependence of H_r. From these simulations we have calculated $|\partial H_r/\partial\phi_H|$ at the two observation frequencies and find the two curves almost identical. Consequently, the term $|\partial H_r/\partial\phi_H|\Delta\phi_H$ from Eq. (12) for $\Delta H_{\mathrm{inhom}}$ has no significant frequency dependence.

Thus, for the rotation of **H** in the plane of this sample, because **M** and **H** are always parallel, ΔH_{hom} will be linearly proportional to the frequency, and $\Delta H_{\mathrm{inhom}}$ will be frequency independent. For this geometry, it then appears appropriate to use the frequency dependence of $\Delta H_{pp}(\omega)$ to separate $\Delta H_{\mathrm{inhom}}$ and ΔH_{hom} from each other, as discussed with Eq. (1). In Fig. 10(a) we display in a polar plot the ϕ_H dependence of the peak-to-peak linewidths at the two frequencies. Using a linear extrapolation to zero frequency for the two linewidths for each value of ϕ_H, one obtains the Gilbert factor G from the slope, and $\Delta H_{\mathrm{inhom}}$ from the intercept. These are plotted as a function of ϕ_H in parts (b) and (c) of Fig. 10, respectively. The Gilbert damping factor G displays an angular symmetry correlated with the crystalline axes. There is a very large variation in the size of G, much larger than any reported by other observers.[8,9] In fact, for certain values of ϕ_H, the parameter G tends to zero.

The results in Fig. 10 (ϕ_H rotation) can be compared with Fig. 9 (θ_H rotation) for self-consistency at the one orientation the two figures have in common the applied field along the in-plane [110] axis. Both sets of data are in agreement that for this orientation of the field, the linewidth is due almost entirely to ΔH_{hom}, with $\Delta H_{\mathrm{inhom}}$ making a negligible contribution. The values of G obtained by the two different fitting procedures are $G=1.50\times10^8$ rad/s (fitting the θ_H dependence at 9.2 GHz) and $G=2.17\times10^8$ rad/s (fitting the ϕ_H dependence with the 9.2 and 4.1 GHz data). The smaller value is about 30% less than the larger. Although the two numbers are in the same ballpark, the discrepancy is larger than the estimated uncertainties in G, the larger being about $\pm10\%$ from the experimental error in the slope of the ΔH_{pp} vs ω curve.

In Fig. 10(c) we have attempted to fit the data for $\Delta H_{\mathrm{inhom}}$ with Eq. (12). The diamonds represent the data, and the solid line is calculated from the equation. The angular dependence of the simulation results from the term $|\partial H_r/\partial\phi_H|\Delta\phi_H$. As can be seen, the data and the simulation show the same angular symmetry, and the overall fit is not too bad. However, in order to obtain the quality of the fit shown, it is necessary to use a value of $\Delta\phi_H=15°$. This number is very much larger than what one anticipates from the quality of the x-ray measurements which were made on the sample.

Looking for other contributions to $\Delta H_{\mathrm{inhom}}$, we examined the consequences of having a spread of values for the constants M, $K_{4\parallel}$, and K_2 in Eq. (9), as well as variations in the parameter $K_{2\parallel}$ (induced by steps on the substrate) and the direction of the steps. Such variations throughout the sample can produce a $\Delta H_{\mathrm{inhom}}$ with the same angular symmetry as seen in Fig. 10(c). A spread of $K_{2\parallel}$ values, for example, is able to account for the differences along the [100] and [110] directions. However, these simulations are in general *out of phase* with the data, in the sense that they give maxima for $\Delta H_{\mathrm{inhom}}$ for those values of ϕ_H at which the data show minima.

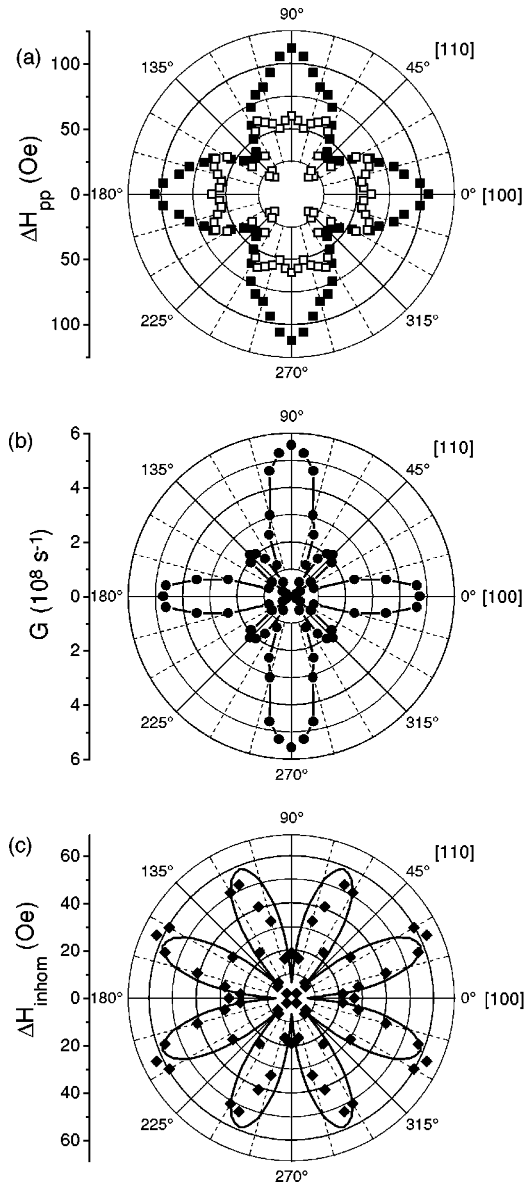

FIG. 10. (a) The peak-to-peak linewidths observed at 4 (open squares) and 9 (solid squares) GHz versus in-plane angle ϕ_H measured from the [100] axis, as displayed on a polar graph. (b) The Gilbert damping factor versus ϕ_H, as determined from the data in part (a). (c) The inhomogeneous contribution to the linewidth versus ϕ_H. The points are obtained from the experimental data in part (a). The line is fitted to the data using Eq. (12) with $\Delta\phi_H=15°$ and $\Delta H_{\mathrm{int}}=0$.

Overall, we have been unable to justify the fitting procedure used for $\Delta H_{\mathrm{inhom}}$ in Fig. 10(c), or to find an alternate procedure which works. Thus, our confidence level in the accuracy of the indicated angular dependence of both $\Delta H_{\mathrm{inhom}}$ and G is not high. Certainly, the frequency and angular dependence of ΔH_{pp} for in-plane rotations is real. The analysis procedure we have used, however, is not consistent with the structural quality of the specimen. Clearly, more experimental and theoretical work is needed for a better interpretation of the ϕ_H dependence of the linewidth data.

V. CONCLUSION

In summary, the FMR linewidth is demonstrated to be an important experimental parameter from which a lot of detailed information on the magnetic and structural state of a ferromagnetic ultrathin film system can be obtained. General trends in the thickness and temperature dependence of the linewidth for several ferromagnetic monolayer systems were discussed, such as a linewidth broadening at lower temperature, due to an increase of the inhomogeneous contribution, and a broadening at all temperatures with decreasing thickness. The latter may result from a change of dimensionality in the thinnest films or, in some cases, to an inhomogeneous contribution arising from an enhanced role of variations of the surface anisotropies. Evidence for an anisotropy of the intrinsic damping (Gilbert parameter) of the magnetization is found in tetragonal Ni/Cu(001) for the first time. Larger damping occurs with **H** parallel to the hard direction, which agrees with observations for Co/Cu(001) (Ref. 19) but is different than the case of Fe films. In Table I we list the narrowest linewidths ΔH_{pp} observed in our studies and compare them to theoretically expected ones using bulk damping parameters. We note that the intrinsic damping, that is G, is enhanced in ultrathin films, in general. A correlation between the experimental ΔH_{pp} and structure must be performed with care, and the film's thickness, temperature, and crystallography must be taken into account. Finally, we have also shown how to distinguish the homogeneous and inhomogeneous linewidths in angular and frequency-dependent measurements. The full analysis is applied to the exemplary case of an Fe_4/V_4 multilayer, where we determined an apparent angular dependence of the Gilbert parameter.

ACKNOWLEDGMENTS

This work was supported in part by the Deutsche Forschungsgemeinschaft, Sfb 290. The $(Fe_4/V_4)_{40}$ sample was prepared at Uppsala University within the Thin Film Consortium.

*Permanent address: Department of Physics and Astronomy, Wayne State University, Detroit, Michigan 48202.

[1] B. Heinrich, in *Ultrathin Magnetic Structures II*, edited by B. Heinrich and J. A. C. Bland (Springer, Berlin, 1994), p. 195.

[2] B. Heinrich and J. F. Cochran, Adv. Phys. **42**, 523 (1993).

[3] M. Farle, Rep. Prog. Phys. (to be published July 1998).

[4] Z. Frait and D. Fraitova, *Spin-Wave Resonance in Metals*, in *Spin Waves and Magnetic Excitations 2*, edited by A. S. Borovik-Romanov and S. K. Schiha (Elsevier Science, Amsterdam, 1988).

[5] J. Pelzl and U. Netzelmann, *Photoacoustic, Photothermal and Photochemical Processes at Surfaces and Thin Films*, Topics in Current Physics Vol. 47 (Springer, Berlin, 1989), p. 313.

[6] Z. Zhang, L. Zhou, P. E. Wigen, and K. Ounadjela, Phys. Rev. Lett. **73**, 336 (1994).

[7] See Hillebrands and Güntherodt (Ref. 1), p. 258.

[8] Z. Celinski and B. Heinrich, J. Appl. Phys. **70**, 5935 (1991).

[9] B. Heinrich, K. B. Urquhart, A. S. Arrott, J. F. Cochran, K. Myrtle, and S. T. Purcell, Phys. Rev. Lett. **59**, 1756 (1987).

[10] J. Heidmann, D. Weller, H. C. Siegmann, and E. L. Garwin, J. Appl. Phys. **79**, 6488 (1996).

[11] H. C. Siegmann, E. L. Garwin, C. Y. Prescott, J. Heidmann, D. Mauri, D. Weller, R. Allenspach, and W. Weber, J. Magn. Magn. Mater. **151**, L8 (1995).

[12] L. He and W. D. Doyle, J. Appl. Phys. **79**, 6489 (1996).

[13] W. Platow, Diploma thesis, Freie Universität Berlin, 1995 (unpublished).

[14] Yi Li and K. Baberschke, Phys. Rev. Lett. **68**, 1208 (1992).

[15] B. Schulz, R. Schwarzwald, and K. Baberschke, Surf. Sci. **307-309**, 1102 (1994).

[16] B. Schulz, Ph.D. thesis, Freie Universität Berlin, 1995 (unpublished).

[17] G. André, A. Aspelmeier, B. Schulz, M. Farle, and K. Baberschke, Surf. Sci. **326**, 275 (1995).

[18] G. André, Diploma thesis, Freie Universität Berlin, 1994 (unpublished).

[19] F. Schreiber, J. Pflaum, Z. Frait, T. Mühge, and J. Pelzl, Solid State Commun. **93**, 965 (1995).

[20] R. J. Elliott, Phys. Rev. **96**, 266 (1954).

[21] S. V. Vonsovskii, *Ferromagnetic Resonance* (Pergamon, Oxford, 1966).

[22] B. Schulz and K. Baberschke, Phys. Rev. B **50**, 13 467 (1994).

[23] M. Farle, B. Mirwald-Schulz, A. N. Anisimov, W. Platow, and K. Baberschke, Phys. Rev. B **55**, 3708 (1997).

[24] M. T. Johnson, P. J. H. Bloemen, F. J. A. de Broeder, and J. J. de Vries, Rep. Prog. Phys. **59**, 1409 (1996).

[25] K. Baberschke, Appl. Phys. A: Mater. Sci. Process. **62**, 417 (1996).

[26] K. Baberschke and M. Farle, J. Appl. Phys. **81**, 5038 (1997).

[27] Yu. V. Goryunov, N. N. Garif'yanov, G. G. Khaliullin, I. A. Garifullin, L. R. Tagirov, F. Schreiber, T. Mühge, and H. Zabel, Phys. Rev. B **52**, 13 450 (1995).

[28] C. Chappert, K. Le Dang, P. Beauvillain, H. Hurdequint, and D. Renard, Phys. Rev. B **34**, 3192 (1986).

[29] M. Farle, M. Zomack, and K. Baberschke, Surf. Sci. **160**, 205 (1985).

[30] M. Farle, A. Berghaus, and K. Baberschke, Phys. Rev. B **39**, 4838 (1989).

[31] M. Farle, A. Berghaus, Yi Li, and K. Baberschke, Phys. Rev. B **42**, 4873 (1990).

[32] Yi Li, M. Farle, and K. Baberschke, J. Magn. Magn. Mater. **93**, 345 (1991).

[33] S. Müller, B. Schulz, G. Kostka, M. Farle, K. Heinz, and K. Baberschke, Surf. Sci. **364**, 235 (1996).

[34] M. Farle, Y. Henry, and K. Ounadjela, Phys. Rev. B **53**, 11 562 (1996).

[35] Yi Li, M. Farle, and K. Baberschke, Phys. Rev. B **41**, 9596 (1990).

[36] F. Spörel and E. Biller, Solid State Commun. **17**, 833 (1975).

[37] A. K. Schmid, D. Atlan, H. Iton, B. Heinrich, T. Ichinokawa, and J. Kirschner, Phys. Rev. B **48**, 2855 (1993).

[38] M. B. Stearns, in *Magnetic Properties of Metals*, edited by H. P. J. Wijn, Landolt-Börnstein, Vol. III/19a (Springer, Berlin, 1986).

[39] M. Farle, W. Platow, A. N. Anisimov, B. Schulz, and K. Baberschke, J. Magn. Magn. Mater. **165**, 74 (1997).

[40] Yi Li, Ph.D. thesis, Freie Universität Berlin, 1991.

[41] G. Dewar, B. Heinrich, and J. F. Cochran, Can. J. Phys. **55**, 821 (1977).

[42] J. L. Bubendorff, J. Pflaum, E. Huebner, D. Raiser, J. P. Bucher, and J. Pelzl, J. Magn. Magn. Mater. **165**, 199 (1997).
[43] M. Farle, W. Platow, A. N. Anisimov, P. Poulopoulos, and K. Baberschke, Phys. Rev. B **56**, 5100 (1997).
[44] J. F. Cochran, J. M. Rudd, M. From, B. Heinrich, W. Bennett, W. Schwarzacher, and W. F. Egelhoff, Jr., Phys. Rev. B **45**, 4676 (1992).
[45] A. Aspelmeier, F. Gerhardter, and K. Baberschke, J. Magn. Magn. Mater. **132**, 22 (1994).
[46] E. D. Tober, R. X. Ynzunza, C. Westphal, and C. S. Fadley, Phys. Rev. B **53**, 5444 (1996).
[47] P. Isberg, B. Hjörvarsson, R. Wäppling, E. B. Svedberg, and L. Hultman, Vacuum **48**, 483 (1997).
[48] P. Poulopoulos, P. Isberg, W. Platow, W. Wisny, M. Farle, B. Hjörvarsson, and K. Baberschke, J. Magn. Magn. Mater. **170**, 57 (1997).
[49] A. N. Anisimov, W. Platow, P. Poulopoulos, W. Wisny, M. Farle, K. Baberschke, P. Isberg, B. Hjörvarsson, and R. Wäppling, J. Phys.: Condens. Matter **9**, 10 581 (1997).
[50] B. Heinrich, C. F. Cochran, M. Kowalski, J. Kirschner, Z. Celinski, A. S. Arrot, and K. Myrtle, Phys. Rev. B **44**, 9348 (1991).
[51] H. Drulis and M. Drulis, in *Magnetic Properties of Rare Earth Elements, Alloys and Compounds*, edited by H. P. J. Wijn, Landolt-Börnstein, Vol. III/19d1 (Springer, Berlin, 1991).